

Nanoscale

Accepted Manuscript



This is an *Accepted Manuscript*, which has been through the Royal Society of Chemistry peer review process and has been accepted for publication.

Accepted Manuscripts are published online shortly after acceptance, before technical editing, formatting and proof reading. Using this free service, authors can make their results available to the community, in citable form, before we publish the edited article. We will replace this *Accepted Manuscript* with the edited and formatted *Advance Article* as soon as it is available.

You can find more information about *Accepted Manuscripts* in the [Information for Authors](#).

Please note that technical editing may introduce minor changes to the text and/or graphics, which may alter content. The journal's standard [Terms & Conditions](#) and the [Ethical guidelines](#) still apply. In no event shall the Royal Society of Chemistry be held responsible for any errors or omissions in this *Accepted Manuscript* or any consequences arising from the use of any information it contains.

ARTICLE

Ultra-broadband unidirectional launching of surface plasmon polaritons by a double-slit structure beyond the diffraction limit

Cite this: DOI: 10.1039/x0xx00000x

Jianjun Chen,^{*ab} Chengwei Sun,^{ab} Hongyun Li^a and Qihuang Gong^{*ab}Received 00th January 2012,
Accepted 00th January 2012

DOI: 10.1039/x0xx00000x

www.rsc.org/

Surface-plasmon-polariton (SPP) launchers, which can couple the free space light to the SPPs on the metal surface, are one of the key elements for the plasmonic devices and nanophotonics systems. Downscaling the SPP launchers below the diffraction limit and directly delivering the SPPs to the desired subwavelength plasmonic waveguides are of importance for high-integration plasmonic circuits. By designing a submicron double-slit structure with different slit widths, an ultra-broadband (>330 nm) unidirectional SPP launcher is realized theoretically and experimentally based on the different phase delays of SPPs propagating along the metal surface and the near-field interfering effect. More importantly, the broadband and unidirectional properties of the SPP launcher are still maintained when the slit length is reduced to a subwavelength scale. This can make the launcher only occupy a very small area of $<\lambda^2/10$ on the metal surface. Such a robust unidirectional SPP launcher beyond the diffraction limit can be directly coupled to a subwavelength plasmonic waveguide efficiently, leading to an ultra-tight SPP source, especially as a subwavelength localized guided SPP source.

1. Introduction

Surface plasmon polaritons (SPPs) are electromagnetic fields propagating along the metal-dielectric interface, and they attract tremendous attention in high-integration photonic circuits because of their subwavelength field confinements and strong field enhancements.¹ However, due to the wave-vector mismatching, the SPPs cannot be directly launched to the smooth metal surface from the free-space light.² Thus, an ultra-small plasmonic structure that can efficiently couple the SPPs from the free-space light to a desired direction or region on the metal surface is very important for the on-chip plasmonic devices. In the past decade, considerable efforts were made to design a variety of plasmonic structures to excite unidirectional SPPs on the metal surface, which could both increase the coupling efficiency and direct the SPPs to the well-defined directions. These plasmonic structures include the slit-grating structure,³ ridge-grating structure,⁴ aperiodic grooves,^{5,6} tilted grating,⁷ interfering nano-structures with different initial phases of the SPPs,^{8,9} compact detuned antennas,¹⁰ waveguide-termination coupling mirrors,¹¹ and even the subwavelength asymmetric nano-slit.^{12,13} By changing the states of the illuminating light, such as the incident angle^{14,15} and polarizations,^{16,17} or using a pump beam,^{18,19} the propagation directions of the generated SPPs can be easily tuned in the metallic-slit structures.¹⁶⁻¹⁹ To realize robust unidirectional SPP launching and satisfy the wide operation bandwidth of plasmonic circuits, broadband unidirectional SPP launchers

have been proposed and demonstrated recently.²⁰⁻²⁵ Using a submicron asymmetric slit coated with a polymer film,²⁰ the bandwidth of > 100 nm for the unidirectional SPPs was achieved experimentally. By designing a submicron groove-doublet structure²¹ or asymmetric optical slot nanoantenna pairs²² on the metal surface, broad bandwidths of >200 nm²¹ or >157 nm²² with high extinction ratios of ≥ 10 dB were obtained. By adopting the chirped plasmonic gratings with a lateral dimension of about $17 \mu\text{m}$ ²³ or $4 \mu\text{m}$,²⁴ the bandwidths of the unidirectional SPP source reached to 190 nm²³ and 210 nm.²⁴ With a pair of phased nanoslits,²⁵ the broadband unidirectional SPPs with a bandwidth of about 300 nm were numerically predicted. While, the generated SPPs from all of these SPP launchers propagated bulkily along the metal surface,^{3-10, 12-25} leading to diverging SPP sources or approximate plane-wave SPP sources on the metal surface.

For the future plasmonic circuits of high integration, it is vital that the unidirectional SPP launchers occupied a very small area beyond the diffraction limit. More importantly, the unidirectional SPPs generated by the ultra-small launcher should be directly and efficiently coupled to a subwavelength plasmonic waveguide rather than bulkily propagate along the metal surface without any confinements. Although some of these unidirectional SPP launchers possessed very small lateral dimensions (parallel to the SPP propagation direction along the metal surface), which can even be downscaled to subwavelength,^{12-14,22,23} nearly all of the unidirectional SPP

launchers had very large longitudinal dimensions ($> 10\lambda$, perpendicular to the SPP propagation direction along the metal surface).^{3-9,12-25} This significantly limits the on-chip integration density of the plasmonic devices. Moreover, the generated SPPs propagated bulkily along the metal surface without any confinements^{3-10,12-25}. This makes it hard to directly couple the generated SPPs to subwavelength plasmonic waveguides. What's worse, the bulky propagation of the SPPs would bring large crosstalk between different plasmonic devices in high-integration plasmonic circuits. Therefore, realizing an efficient unidirectional SPP launcher with small occupied areas beyond the diffraction limit on the metal surface and meanwhile coupling the SPPs directly to a subwavelength plasmonic waveguide are an enormous challenge.

In the letter, we design a submicron double-slit structure on the metal surface, which comprises two nano-slits of different slit widths on the metal surface. Different from the previous phased nanostructures,^{8-10,15,21,22,25} the two slits in the double-slit structure generate the SPPs of nearly equal amplitudes and initial phases. Based on the different phase delays of SPPs propagating along the metal surface and the near-field interfering effect in the submicron double-slit structure, an ultra-broadband SPP launcher is realized theoretically and experimentally. The bandwidth is larger than 330 nm, which is greater than that in the previous structures.²⁰⁻²⁵ Moreover, its broadband and efficient properties are still maintained when the slit length is reduced to a subwavelength scale ($< \lambda/10$), which is about one hundred times smaller than that in the previous unidirectional SPP launchers.^{3-9,12-25} This significantly shrinks the occupied area of the SPP launcher on the metal surface to be smaller than $\lambda^2/10$. To avoid the bulky propagation of the SPPs along the metal surface, such a robust unidirectional SPP launcher beyond the diffraction limit is directly coupled to a subwavelength plasmonic waveguide. Therefore, the double-slit structure beyond the diffraction limit can act as an ultra-small SPP source, especially as a subwavelength localized guided SPP source, which has many important applications in high-integration plasmonic circuits.

2. Simulation results of the double-slit structure

The proposed double-slit structure is schematically shown in Fig. 1(a), which comprises only two nano-slits with different slit widths (w_1 and w_2). Here, the slit length (perpendicular to the x - y plane) is assumed to be infinite.

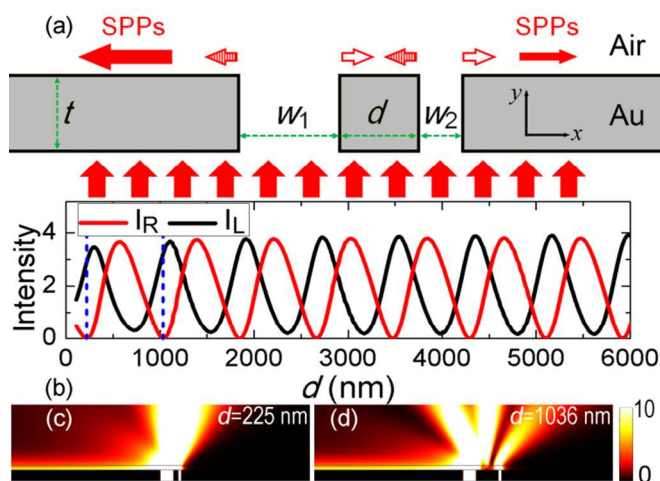


Fig. 1 Unidirectional SPP launching in the double-slit structure. (a) Schematic and geometry parameters of the double-slit structure. (b) Intensity of the SPPs generated by the metallic double-slit structure for different slit separations when $w_1=600$ nm and $w_2=140$ nm. Field distributions of the power flow in the double-slit structure for (c) $d=225$ nm and (d) $d=1036$ nm.

It is well known that Yong's double-slit structure of equal slit widths is very famous and its far-field interfering pattern is usually used to demonstrate the wave nature of light. In the letter, we mainly focus on the near-field SPPs generated by the metallic double-slit structure on the front metal surface. When a p-polarized beam illuminates the double-slit structure from the back side, each slit acts as a SPP source, which can launch two equal SPPs propagating to the opposite directions on the metal surface, as shown by the half-hollow and hollow red arrows. In each direction, the SPPs generated by the two slits will interfere with each other. This interference will greatly manipulate the SPP intensities away from the double-slit structure, as shown by the solid red arrows.

It is easy to obtain that the interfering SPPs (coming from the two slits) in the right and left directions have phase differences of

$$\begin{cases} \Phi_R = \frac{2\pi}{\lambda} n_{\text{eff}} d + \frac{2\pi}{\lambda} w_2 + \varphi \\ \Phi_L = \frac{2\pi}{\lambda} n_{\text{eff}} d + \frac{2\pi}{\lambda} w_1 - \varphi \end{cases}, \quad (1)$$

where, the subscripts of R and L denote the right and left propagation directions of the SPPs, respectively; n_{eff} is the effective refractive index of the SPPs propagating along the air-metal interface; d is the separation of the double slits; and φ equals $\varphi_1 - \varphi_2$, in which φ_1 and φ_2 are the sum of the phase shifts brought by the light propagating through the Slit 1 and Slit 2, the SPP excitation at the Slit 1 and Slit 2, and the SPPs transmitting through the edges of the Slit 2 and Slit 1. It is noted that w_1 and w_2 are independent in Eq. (1). Thus, the conditions of both $\Phi_R = (2m+1)\pi$ and $\Phi_L = (2m'+2)\pi$ (where $m=0, 1, 2, \dots$ and $m'=0, 1, 2, \dots$) can be easily satisfied by choosing different values of w_1 and w_2 . When the separation of the double slits (d) is fixed, the values of w_1 and w_2 are determined by

$$\begin{cases} w_1 = \frac{(2m'+2)\pi + \varphi}{2\pi} \lambda - n_{\text{eff}} d \\ w_2 = \frac{(2m+1)\pi - \varphi}{2\pi} \lambda - n_{\text{eff}} d \end{cases}, \quad (2)$$

In this case, completely destructive interferences for the right-propagating SPPs and completely constructive interferences for the left-propagating SPPs will occur if the interfering SPPs have equal amplitudes. Simulations with Comsol Multiphysics show that the condition of equal amplitudes for the interfering SPPs can also be easily obtained by using different slit widths (Figure S1 in Supplementary Information). Thus, the slit widths can manipulate both of the phase differences and amplitudes of the interfering SPPs in the double-slit structure. By choosing proper slit widths, an efficient unidirectional SPP launcher of high extinction ratios can be achieved in the double-slit structure.

To demonstrate our proposal, the SPP intensities excited by the double-slit structure are calculated by varying the slit separation of d (ranging from 100 nm to 6000 nm), and the

results are shown in Fig. 1(b). Here, the double-slit structure on a 500-nm-thick gold film is illuminated by a plane-wave p-polarized beam of $\lambda=830$ nm from the back side. In the simulation, the permittivity of the air and gold are set to $\epsilon_{\text{Air}}=1.0$ and $\epsilon_{\text{Au}}=-26.61+1.665i$ at $\lambda=830$ nm,²⁶ respectively. When the slit widths are set to be $w_1=600$ nm and $w_2=140$ nm, the two interfering SPPs in the right direction have equal amplitudes. This can result in a completely destructive interference of the SPPs in the right direction when $\Phi_R=(2m+1)\pi$, such as $I_R\approx 0.001$ for $d=1036$ nm, as shown by the red line in Fig. 1(b). Meanwhile, nearly completely constructive interference is obtained in the left direction ($I_L\approx 3.3$ for $d=1036$ nm), as shown by the black line in Fig. 1(b). This agrees well with our analysis above. Herein, the SPP intensity generated by the double-slit structure is normalized to that in the single nanoslit with a width of $w=140$ nm. Simulations show that similar results can be obtained by normalizing the SPP intensity to that in the wide slit because the narrow and wide slits can generate the SPPs with nearly equal intensities (Figure S1 in Supplementary Information).

From Fig. 1(b), it is obviously observed that the curves exhibit periodic oscillation behaviours, and the period referring to the separation of d is $P=814$ nm $\approx \lambda_{\text{SPP}}=[(\epsilon_{\text{Air}}+\epsilon_{\text{Au}})/(\epsilon_{\text{Air}}\epsilon_{\text{Au}})]^{1/2}$. This matches well with the value of $\Delta d=\lambda_{\text{SPP}}$ inferring from Eq. (1). Typical power flow distributions with $d=225$ nm and $d=1036$ nm are presented in Fig. 1(c,d). It is clearly observed that the SPPs generated by the double-slit structure mainly propagate to the left direction. For the right direction, the SPPs are completely vanished, and the extinction ratio can reach up to $10\times\log(I_L/I_R)\approx 35$ dB for $d=1036$ nm. Therefore, efficient unidirectional SPP launching is successfully realized in the simple double-slit structure by using different slit widths. Besides, it is found that the decreasing of w_1 and increasing of w_2 would increase the SPP launching efficiency but decrease the extinction ratio. Since the propagation constant of the SPPs in the metal slit is insensitive to the wavelengths and the slit width when the slit width is greater than 100 nm, the thickness of the metal film (t) nearly has no influence on the unidirectional SPP launcher.

Based on Eq. (1), the variation of Φ_R induced by changing the incident wavelengths is $\Delta\Phi_R\approx 2\pi[(d+w_2)/\lambda^2]\Delta\lambda$. When $d+w_2$ is much smaller than λ , $\Delta\Phi_R$ is varied slightly when changing the incident wavelength ($\Delta\lambda$), indicating that Φ_R is insensitive to the incident wavelength. Thus, to achieve a broadband unidirectional SPP launcher, the smallest separation ($d_{\text{min}}=225$ nm) should be chosen, as shown by the left dashed line in Fig. 1(b). In this case, the unidirectional SPP launcher possesses the smallest lateral dimension of 965 nm. To present this phenomenon, the SPP intensities generated by such a submicron double-slit structure at the wavelengths ranging from 700 nm to 1100 nm are calculated, and the results are displayed in Fig. 2(a). Herein, the permittivity of gold as a function of λ is taken from the experiment results²⁶ and expanded by using the method of interpolation. It is observed that the intensity of the left-propagating SPPs is much greater than that of the right-propagating SPPs in the investigated wavelength range. Hence, the SPPs mainly propagate to the left direction for a broad bandwidth, and the bandwidth is greater than 330 nm based on the definition in Ref. [21,22,25], where the extinction ratio is greater than 10 dB. At $\lambda=835$ nm, the extinction ratio can reach up to $10\times\log(I_L/I_R)\approx 39$ dB. Moreover, the intensity of the generated SPPs is greater than 2 in this bandwidth, as shown by the black line in Fig. 2(a). The coupling efficiency, which is defined as the quotient of the

power flows between the generated SPPs and the incident beam, is strongly depends on the spot size of the focused laser beam. For a given focused spot size of the incident laser, such as 1.1 μm ,¹¹ the actual value of the coupling efficiency is about 5% in the submicron double-slit structure. Simulation shows that the generated SPP intensity with such a tightly focused laser beam only decreases to about 81% of that by using the plane-wave incidence. This mainly attributes to the submicron dimension of the double-slit structure. This also reveals the robust realization of the unidirectional SPP launcher.

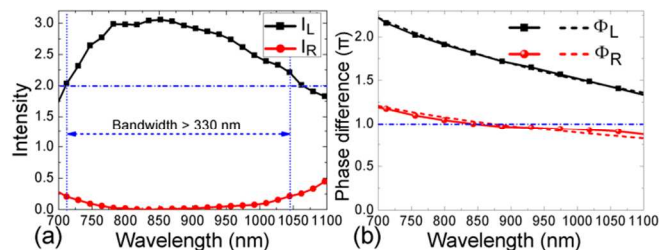


Fig. 2 Ultra-broadband unidirectional SPP launching and the phase analysis. (a) Intensities of the generated SPPs at different wavelengths. (b) Phase differences of the interfering SPPs (generated by the two slits) in the left and right directions. The solid symbol lines are the simulation results, while the dashed lines are the calculated results based on Eq. (1).

To further understanding the underlying physics of the ultra-broadband unidirectional SPPs in the submicron double-slit structure, the phase differences of the interfering SPPs generated by the two slits in the two directions are calculated, and the results are shown by the solid lines in Fig. 2 (b). The phase differences of the interfering SPPs based on Eq. (1) are also given by the dashed lines in Fig. 2(b), where $\varphi=0.15\pi$. It is noted the agreement between them is excellent. For the left-propagating SPPs, it is observed that Φ_L varies from 2.2π to 1.3π when changing λ (black lines in Fig. 4b), and the constructive interference can occur at most of the wavelengths in the investigated range. Hence, the intensity is greater than 1.8 in the investigated wavelength range, as shown by the black line in Fig. 2 (a). For the right direction, $d+w_2$ is only about 365 nm, which is much smaller than the incident wavelength. This is near-field interference, and thus it is difficult for the right-going SPPs to accumulate enough phase differences. This makes the phase difference of Φ_R being insensitive to the incident wavelength, so the value of Φ_R is nearly equal to π in the investigated wavelengths, as shown by the red lines in Fig. 2(b). Moreover, the amplitudes of the interfering SPPs in the right direction are comparable [Figure S2(b) in Supplementary Information]. Based on the interference condition, nearly completely destructive interferences can be obtained for the right-propagating SPPs in the investigated wavelength range. This results in the intensity being very small ($I < 0.5$), as shown by the red line in Fig. 2(a). Therefore, the SPPs generated by the submicron double-slit structure mainly propagate to the left direction for a broad bandwidth, revealing an ultra-broadband and efficient unidirectional SPP launcher.

3. Experimental demonstration of the ultra-broadband SPP launcher

In the following, we further demonstrate our proposal experimentally. The submicron double-slit structure is fabricated using focused ion beams (FIB) in a 450-nm-thick gold film, which is evaporated on a glass substrate with a 30-

nm-thick titanium adhesion layer. Fig. 3(a) shows the scanning electron microscopy (SEM) image of the experimental sample on a gold film. The compact double-slit structure is located on the lower and middle part of the image. Fig. 3(b) displays the details of the double-slit structure. The measured geometrical parameters of the double-slit structure are as follows: the widths of Slit 1 and Slit 2 are about $w_1=580$ nm and $w_2=160$ nm; the separation of the two slits is about $d=200$ nm; and the length of the slits is about $L_{\text{slit}}=10$ μm . So, the total lateral dimension of the double-slit structure is only about 940 nm. On the two sides of the image, two decoupling gratings (period of 760 nm and separation of about 30 μm) are fabricated to scatter the SPPs for the far-field detection. In this experimental configuration, it is difficult to measure the coupling efficiency of the double-slit structure because the decoupling efficiency of the gratings cannot be obtained in the experiment. To address the problem, an in-chip reference slit of $w=160$ nm is fabricated on the upper lower and middle part of the image in Fig. 3(a), which allows us to directly compare the measured results with the simulation results (without measuring the decoupling efficiency). Moreover, the laser power fluctuation and the dependence of the detector sensitivity on the wavelengths can be eliminated in the experiment.

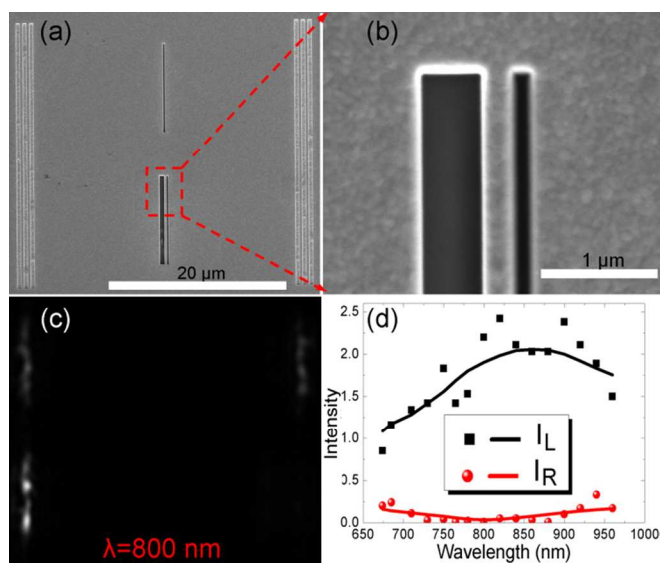


Fig. 3 Experimental demonstration of ultra-broadband unidirectional SPP launching in the submicron double-slit structure. (a) SEM image of the experimental sample. (b) Details of the double-slit structure. (c) CCD pictures of the scattered light from the decoupling gratings at $\lambda=800$ nm. (d) SPP intensities measured at different incident wavelengths. The black and red solid lines are obtained by smoothing the experimental results.

In the experiment, the experimental sample is normally illuminated from the back side using a p-polarized laser beam (Ti:sapphire laser) with a radius of about 100 μm , which could ensure nearly uniform incident intensities over the slits and avoid the noise of the incident light. The generated SPPs propagate along the front metal surface and then are scattered by the decoupling gratings. The scattered light is collected by a long working distance objective (Mitutoyo 50 \times NA=0.42) and then is imaged onto a charge coupled device (CCD). In the CCD pictures, it is observed that the signal intensities scattered from the upper part of the two decoupling gratings are nearly the same because the referenced nano-slit is a symmetric

structure. However, for the lower part of the two decoupling gratings, the phenomenon becomes quite different. It is observed that the lower half part of the right decoupling grating is very dark for a large incident wavelength range, while the lower half part of the left decoupling grating is very much brighter than the upper part. One typical CCD picture at the wavelength of $\lambda=800$ nm is displayed in Fig. 3(c). Here, the strong light transmitted from the middle nano-slits is blocked by a diaphragm, and only the scattered light from the decoupling gratings is imaged on CCD. The CCD picture obviously shows that the generated SPPs propagate to the left direction efficiently. Fig. 3(d) shows the measured SPP intensities for various incident wavelengths. Here, the SPP intensity, I , is obtained from the quotient between the light intensities scattered from the lower and the upper parts of the decoupling grating (evaluated by integration over a spatial scale on the grating). The measurement of the relative SPP intensities^{3,6-10,12-25} can eliminate the laser power fluctuation as well as the dependence of the detector sensitivity and decoupling efficiency on the wavelengths in the experiment. Moreover, we can compare the measured results with the calculated results directly.

It is noted that the SPPs in the left direction is always much greater than that in the right direction, revealing ultra-broad and efficient unidirectional SPP launching in the submicron double-slit structure. This results match well with the simulation results in Fig. 2(a). The slight differences between the experimental and simulation results are mainly attributed to the imperfect fabrications [Fig. 3(a,b)] and the structural dimensional deviation. But the ultra-broadband unidirectional SPP launching is obviously observed, indicating the robust realization of the unidirectional SPP launching in such a small structure. Further simulations show that the slight fabrication deviation of 10% in the double-slit structure can be accepted for realizing the broadband unidirectional SPP launching. Therefore, by engineering the slit widths in the submicron double-slit structure, the ultra-broadband and efficient unidirectional SPP launcher is successfully realized in the experiment.

4. Downscaling the unidirectional SPP launcher below the diffraction limit on a subwavelength plasmonic waveguide

For this SPP launcher, the slit is still very long ($L_{\text{slit}}>10\lambda$), which greatly limits its integration density in the future plasmonic circuits. Moreover, the generated SPPs propagate bulkily along the metal surface, just like the previous structures.^{3-10, 12-25} This will bring large crosstalk to other on-chip plasmonic devices on the metal surface. This also makes it difficult to couple the SPPs directly and efficiently to subwavelength plasmonic waveguides. Fortunately, it is found that the ultra-broadband properties of the SPP launcher are still maintained when the slit length is reduced to a subwavelength scale, as schematically shown in Fig. 4(a). Here, the slit length of the double-slit structure is reduced to be $L_{\text{slit}}=240$ nm, so the unidirectional SPP launcher occupy a very small area of about $\lambda^2/3$ on the metal surface. To realize subwavelength confinements of the SPPs for potential applications in highly integrated plasmonic circuits, the shortened double-slit structure is directly coupled to a subwavelength plasmonic waveguide, as shown in Fig. 4(a). The inset in Fig. 4(a) presents the sectional view of the plasmonic waveguide, which consists of a metal strip with a cross-section dimension of

240×300 nm² on the 200-nm-thick gold film. The field distributions of the SPPs generated by this structure are simulated and the results are shown in Fig. 4(b), where the SPPs are mainly coupled to the left subwavelength plasmonic waveguide at $\lambda=830$ nm. The inset in Fig. 4(b) displays the field distribution of the SPP mode in the plasmonic waveguide, revealing a well confinement of the SPPs (mode size of about 400 nm) by the subwavelength metal ridge. More simulations show that the unidirectional launching properties of the SPP launcher can be obtained when the slit length is further reduced, such as $L_{\text{slit}}=70$ nm (Figure S3 in Supplementary Information). In this case, the occupied area of the unidirectional SPP launcher can be downscaled to be 0.067 μm^2 , which is smaller than $\lambda^2/10$. This significantly downscales the SPP launcher below the diffraction limit.

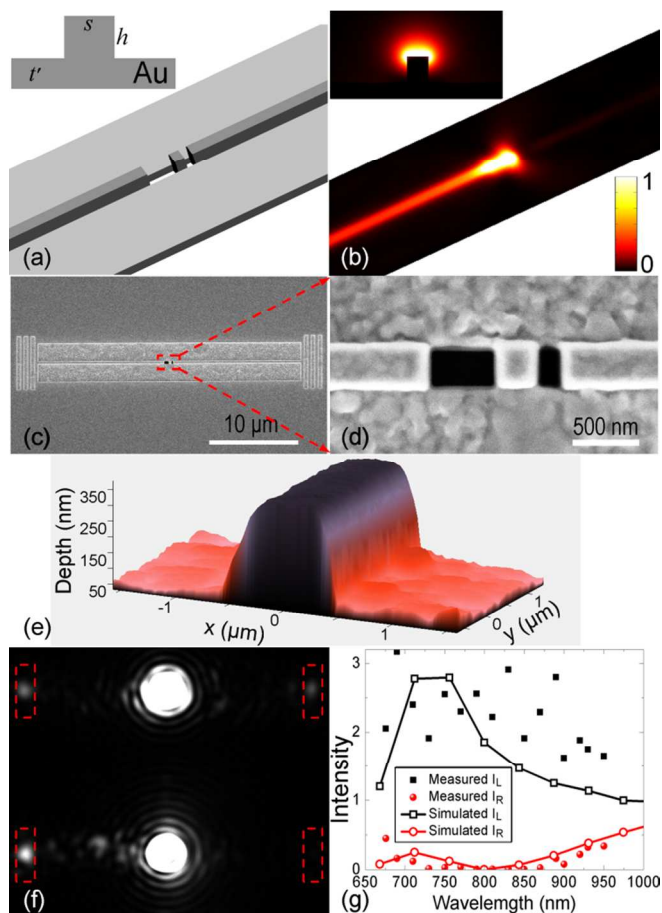


Fig. 4 Downscaling the unidirectional SPP launcher below the diffraction limit and directly coupling the generated SPPs to a subwavelength plasmonic waveguide. (a) Schematic structure of the shortened double-slit structure directly coupled with a subwavelength plasmonic waveguide. Inset shows the sectional view of the subwavelength plasmonic waveguide, where $s=L_{\text{slit}}=240$ nm, $h=300$ nm and $t'=200$ nm. (b) Field distribution (power flow) of the shortened double-slit structure 100 nm above the subwavelength plasmonic waveguide. Inset shows the field distribution of the SPP mode supported by the subwavelength plasmonic waveguide. The SPP mode has an effective refractive index of $n_{\text{eff}}\approx 1.04$ and a propagation length of $L_{\text{SPP}}\approx 20$ μm . (c) SEM image of the experimental sample. (d) Details of the shortened double-slit structure coupled with a subwavelength plasmonic waveguide. (e) AFM image of the subwavelength plasmonic waveguide. (f) CCD pictures of the

scattered light from the experimental sample (down) and the reference sample (top). (g) Measured (dots) and simulated (solid lines) results of the SPP intensity at different wavelengths.

Experimentally, such a shortened double-slit structure beyond the diffraction limit is fabricated by the focused ion beams on the metal surface, as shown in Fig. 4(c). We first fabricate the subwavelength plasmonic waveguide by etching two 300-nm-deep rectangles with a length of 30 μm and a width of 2 μm on the gold film, leaving a metal strip, as shown in Fig. 4(c). Then, the shortened double-slit structure is etched in the subwavelength plasmonic waveguide. Last, two decoupling gratings with lengths of about 6 μm are fabricated at the end of the subwavelength plasmonic waveguide. The details of the structure are displayed in Fig. 4(d). The measured structural parameters are about $w_1=550$ nm, $w_2=120$ nm, $d=250$ nm, and $L_{\text{slit}}=280$ nm. So the SPP launcher occupies a very small area of only about 0.26 μm^2 , which equals about $\lambda^2/3$. Fig. 4(e) displays the atomic force microscope (AFM) image of the subwavelength plasmonic waveguide on the metal surface, and the measured height of the plasmonic waveguide is about 300 nm. Thus, the metal strip in the plasmonic waveguide has a cross-section dimension of about 280×300 nm². An on-chip reference structure which only comprises a single shortened slit with a width of $w=550$ nm and a length of $L_{\text{slit}}=280$ nm in the plasmonic waveguide is also fabrication (Figure S5 in Supplementary Information). Under the illumination of a bulky p-polarization light, a bright spot is clearly observed on the left grating in the CCD picture, while the right grating is nearly dark, as shown by Fig. 4(f). In addition, it is noted that the area of the bright spot is much smaller than that of the decoupling grating [the red dashed rectangle in Fig. 4(f)]. While, without the coupling plasmonic waveguide, the whole decoupling gratings are lit up in the CCD pictures (Figure S6 in Supplementary Information). Hence, in our investigated sample [Fig. 4(c)], the generated SPPs are efficiently coupled to the subwavelength plasmonic waveguide in the left direction, indicating a strongly localized guide SPP source. The SPP intensity for the two directions at different incident wavelengths is also measured, and the results are shown by the dots in Fig. 4(g). These results match well with the simulation results [solid lines in Fig. 4(g)]. Therefore, the ultra-broadband and efficient properties of the unidirectional launcher are still maintained when the slit length is reduced to a subwavelength scale, and the generated SPPs can be directly coupled to the subwavelength plasmonic waveguide. Although the conventional laser is used in the experiment, this subwavelength SPP launcher shows potential applications in the area of integrated a nanolaser^{27,28} or a nano source²⁹ with a subwavelength waveguide, which can considerably improve the degree of integration in the future nano-plasmonic circuits.

5. Conclusions

By using the submicron double-slit structure, the ultra-broadband unidirectional SPP launcher was demonstrated theoretically and experimentally. The phase differences and amplitudes of the interfering SPPs in the double-slit structure could be engineered by the slit widths simultaneously. As a result, an ultra-broadband (>330 nm) unidirectional SPP launcher was realized in the submicron double-slit structure. More importantly, its ultra-broadband and efficient properties were still maintained when the slit length was reduced to a subwavelength scale. This could significantly shrink the

occupied area of the launcher on the metal surface to be smaller than $\lambda^2/10$. Moreover, the ultra-broadband unidirectional SPP launcher could be directly coupled to the subwavelength plasmonic waveguide. Such a robust unidirectional SPP launcher beyond the diffraction limit can act as an ultra-small SPP source, especially as a subwavelength localized guided SPP source. Therefore, it may find important applications in broadband and high-integration plasmonic circuits. The engineering of amplitudes and phase differences of the SPPs with slit widths in the subwavelength plasmonic waveguide may pave new route to manipulating the light at the subwavelength scales.

Acknowledgements

This work was supported by the National Basic Research Program of China (Grants 2013CB328704) and the National Natural Science Foundation of China (Grants 11204018 and 11134001).

Notes and references

^a State Key Laboratory for Mesoscopic Physics and Department of Physics, Peking University, Beijing 100871, China. E-mail: jjchern@pku.edu.cn; qhong@pku.edu.cn

^b Collaborative Innovation Center of Quantum Matter, Beijing, China.

Electronic Supplementary Information (ESI) available: [Intensities of the SPPs generated by a single nano-slit, amplitudes of the magnetic field as one slit being illuminated, the unidirectional SPP launcher of $<\lambda^2/10$, white beam illumination experiment, on-chip reference structure, and diverging SPP source without coupling plasmonic waveguides]. See DOI: 10.1039/b000000x/.

- D. K. Gramotnev and S. I. Bozhevolnyi, *Nat. Photonics*, 2010, **4**, 83-91.
- Z. H. Han and S. I. Bozhevolnyi, *Rep. Prog. Phys.*, 2013, **76**, 016402.
- F. Lopez-Tejiera, S. G. Rodrigo, L. Martin-Moreno, F. J. Garcia-Vidal, E. Devaux, T. W. Ebbesen, J. R. Krenn, I. P. Radko, S. I. Bozhevolnyi, M. U. Gonzalez, J. C. Weeber, and A. Dereux, *Nat. Phys.*, 2007, **3**, 324-328.
- I. P. Radko, S. I. Bozhevolnyi, G. Brucoli, L. Martin-Moreno, F. J. Garcia-Vidal, and A. Boltasseva, *Opt. Express*, 2009, **17**, 7228-7232.
- A. Baron, E. Devaux, J. C. Rodier, J. P. Hugonin, E. Rousseau, C. Genet, T. W. Ebbesen, and P. Lalanne, *Nano Lett.*, 2011, **11**, 4207-4212.
- X. P. Huang and M. L. Brongersma, *Nano Lett.*, 2013, **13**, 5420-5424.
- L. Wang, T. Li, L. Li, W. Xia, X. G. Xu, and S. N. Zhu, *Opt. Express*, 2012, **20**, 8710-8717.
- G. Lerosey, D. F. P. Pile, P. Matheu, G. Bartal, and X. Zhang, *Nano Lett.*, 2009, **9**, 327-331.
- T. Xu, Y. H. Zhao, D. C. Gan, C. T. Wang, C. L. Du, and X. G. Luo, *Appl. Phys. Lett.*, 2008, **92**, 101501.
- Y. Liu, S. Palomba, Y. Park, T. Zentgraf, X. Yin, and X. Zhang, *Nano Lett.*, 2012, **12**, 4853-4858.
- C. L. C. Smith, A. H. Thilsted, C. E. Garcia-Ortiz, I. P. Radko, R. Marie, C. Jeppesen, C. Vannahme, S. I. Bozhevolnyi, and A. Kristensen, *Nano Lett.* 2014, **14**, 1659-1664.
- J. J. Chen, Z. Li, S. Yue, and Q. H. Gong, *Appl. Phys. Lett.*, 2010, **97**, 041113.
- D. D. Li, D. H. Zhang, C. C. Yan, T. Li, Y. K. Wang, Z. J. Xu, J. Wang, and F. Qin, *Opt. Express*, 2013, **21**, 5949-5956.
- B. Wang, L. Aigouy, E. Bourhis, J. Gierak, J. P. Hugonin, and P. Lalanne, *Appl. Phys. Lett.*, 2009, **94**, 011114.
- X. W. Li, Q. F. Tan, B. F. Bai, and G. F. Jin, *Appl. Phys. Lett.*, 2011, **98**, 251109.
- F. J. Rodriguez-Fortuno, G. Marino, P. Ginzburg, D. O'Connor, A. Martinez, G. A. Wurtz, and A. V. Zayats, *Science*, 2013, **340**, 328-330.
- J. Lin, J. P. B. Mueller, Q. Wang, G. H. Yuan, N. Antoniou, X. C. Yuan, and F. Capasso, *Science*, 2013, **340**, 331-334.
- J. J. Chen, Z. Li, S. Yue, and Q. H. Gong, *Nano Lett.*, 2011, **11**, 2933-2937.
- J. J. Chen, Z. Li, X. Zhang, J. H. Xiao, and Q. H. Gong, *Sci. Rep.*, 2013, **3**, 1451.
- J. J. Chen, Z. Li, M. Lei, S. Yue, J. H. Xiao, and Q. H. Gong, *Opt. Express* 2011, **19**, 26463-26469.
- H. Liao, Z. Li, J. Chen, X. Zhang, S. Yue, and Q. Gong, *Sci. Rep.*, 2013, **3**, 1918.
- J. Yang, X. Xiao, C. Hu, W. Zhang, S. Zhou, and J. Zhang, *Nano Lett.*, 2014, **14**, 704-709.
- J. S. Bouillard, S. Vilain, W. Dickson, G. A. Wurtz, and A. V. Zayats, *Sci. Rep.*, 2012, **2**, 829.
- C. C. Lu, X. Y. Hu, H. Yang, and Q. H. Gong, *Adv. Opt. Mater.*, 2013, **1**, 792-797.
- C. H. Gan and G. R. Nash, *Opt. Lett.*, 2013, **38**, 4453-4456.
- P. B. Johnson and R.-W. Christy, *Phys. Rev. B*, 1972, **6**, 4370.
- M. A. Noginov, G. Zhu, A. M. Belgrave, R. Bakker, V. M. Shalaev, E. E. Narimanov, S. Stout, E. Herz, T. Suteewong, and U. Wiesner, *Nature*, 2009, **460**, 1110-1112.
- R. F. Oulton, V. J. Sorger, T. Zentgraf, R. M. Ma, C. Gladden, L. Dai, G. Bartal, and X. Zhang, *Nature*, 2009, **461**, 629-632.
- Y. C. Jun, K. C. Y. Huang, and M. L. Brongersma, *Nat. Commun.*, 2011, **2**, 283.